# Computational Zoning of Unconventional Aircraft

## S Austin*, C Guerra-Garcia*, J Peraire*

*Department of Aeronautics and Astronautics, Massachusetts Institute of Technology, Cambridge, MA, USA 02139

austinsp@mit.edu, guerrac@mit.edu

## 1. ABSTRACT

The protection of aircraft from lightning strikes, both triggered and intercepted, is an essential component in the aircraft development and certification process. In the past, lighting strikes to aircraft have caused catastrophic accidents that have promoted extensive studies into the mechanisms behind lightning events and their mitigation strategies. These recommendations have led to protective measures in the form of wire mesh and diverter strips on nonmetallic surfaces, removing sources of spark-triggered ignition in the fuel system, adequate grounding and wire bundle shielding strategies, and route management to avoid thunderstorms.

While significant progress has been made in aircraft lighting protection, much of what we know about aircraft triggered lightning comes from historical experience and testing. Next generation aircraft designs may not conform to the same assumptions under which models for existing aircraft are valid.

We present a general computational tool for the prediction of the first and second attachment points on arbitrary aircraft geometries. The tool couples numerical electrostatics simulation to a predictive attachment model, and uses open source software which is freely available. The attachment model follows similar methods developed by Onera and the University of Padova in the 1990s, but accounts for both positive and negative first leader inception. Additionally, a feature to determine the optimal aircraft charge has been incorporated into the tool, following prior work by our team on triggered-lightning risk-reduction measures. The tool will be demonstrated by application to the MIT D8 "Double Bubble" aircraft.

## 2. INTRODUCTION

Lightning has long posed a threat to aviation through direct and indirect effects of strikes to aircraft, schedule delays, and costly route modifications to avoid thunderstorms [1,2]. Significant energy has been expended in recent decades to study and mitigate the problem [3]. With an increasing reliance on computation, new tools are being developed to understand and predict aircraft triggered lightning more accurately than past models that relied on similarity with previously qualified designs [4,5,6]. The aircraft of tomorrow will look significantly different from those currently operating, both in form and in function. For example, substantial interest has been generated recently in Urban Air Mobility and Vertical Take-Off and Landing (VTOL) vehicles. Additionally, the design of commercial air transports is being re-evaluated to reduce noise, emissions, and fuel burn. In many circumstances, these aircraft bear little resemblance to existing designs, or they incorporate features that would cause them to need to be re-zoned [6]. In these circumstances, a 21st century zoning solution is required to treat such unconventional geometries. Here, we develop a new computational tool for the automatic zoning assessment of new aircraft. The tool can be run without any *a priori* knowledge of aircraft attachment points, as such knowledge is assumed not to be available.

The phenomenological description of lighting strikes to aircraft is based on the uncharged bidirectional leader theory of Kasemir [7]. In this theory, the conductive aircraft body, when placed in an external electric field, becomes polarized. The polarization leads to charge buildup at opposed ends of the aircraft, which amplifies the local electric field at regions with a small radius of curvature. When the local field becomes strong enough, a streamer corona can form that triggers leader inception if certain criteria are met. The positive leader is typically incepted first, which is followed milliseconds later by the negative leader, as positive charge is removed during propagation of the initial leader. Electrostatic models coupled to simplified models of leader inception can be used to predict the spatial attachment probability of first and second leader inception. These models were first developed by Onera in the 1990s but did not become popular as there was little motivation to invest back then, and the criteria for leader inception did not allow for quantitative agreement. The new landscape of aircraft and advancements in gas discharge physics motivates revisiting these models now.

## 3. MODEL

The zoning assessment is performed by first determining the prestrike electrical environment for any orientation of the aircraft, relative to the ambient electric field, and net surface charge. Then, semi-empirical correlations are applied that model the detailed gas-discharge physics leading to leader inception under the applied fields.

The computational model uses Laplace's equation to solve for the pre-strike electrical environment on the exterior of the aircraft:

$$\nabla^2 \Phi = 0 \qquad (1)$$

This model assumes the absence of space charge around the aircraft. The space charge, which plays a role in the streamer and leader inception process, is modeled through correlations after the electrostatic solution is obtained. Such an approach is used by others in the literature, for example [3,4,8]

The linearity of (1) allows for the electrostatic solution at an arbitrary orientation and aircraft charge to be calculated by taking linear combinations of four basis solutions with different boundary conditions ($\mathbf{E_x}$, $\mathbf{E_y}$, $\mathbf{E_z}$, and $\mathbf{E_Q}$). The first three indicate the electrostatic solution under a homogeneous aircraft charge, with the field pointing along one of the three cardinal directions. $\mathbf{E_Q}$ corresponds to a non-zero aircraft net charge with zero ambient electric field. The coordinate system for the problem is set up as follows:

*Figure 1. Coordinate system for the problem. Model aircraft is the MIT D8, to be discussed in Section 5.*

In this coordinate system, the total electric field can be calculated as:

$$E = \frac{Q_{ac}}{C} E_Q + E_\infty \big( sin(\theta)cos(\phi)E_x + sin(\theta)sin(\phi)E_y + cos(\theta)E_z \big) \tag{2}$$

Where:

- C is the aircraft capacitance, calculated numerically
- $Q_{ac}$ is the aircraft net charge
- $(\theta, \phi)$ represent the orientation of the aircraft, in the frame of Fig. 1.

The electrostatic solutions ($E_x$, $E_y$, $E_z$, and $E_Q$) are obtained numerically with a Galerkin Finite Element code written for this application. The code is written in Python, supports open source mesh generation and visualization plugins, and can support meshes with up to 10 million tetrahedral elements [9,10].

## 4. LEADER INCEPTION CRITERIA

Simulating the detailed leader inception physics discussed in the previous section requires knowledge of the thermodynamic and hydrodynamic environment near the aircraft on very short time scales. However, simplified models make use of the critical charge concept, which relates the amplitude of the electric field to the ability to incept a leader [11, 12]. A leader can be incepted if the corona charge exceeds the critical charge, which depends on the leader sign.

### 4.1 Calculation of the corona charge

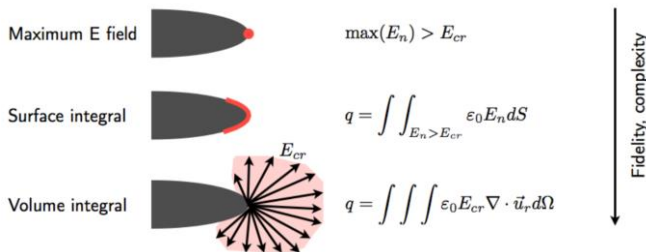Calculation of the corona charge is performed by one of the following three methods:



*Figure 2. Corona inception criteria based on three critical charge calculation methods*

The simplest approach indicates an incepted leader when the normal electric field at a point on the aircraft surface exceeds the corona stabilization value $E_{cr}$. However, this method can exhibit a dependence on the mesh, especially on coarser meshes. As such, the surface and volume integral methods are preferred.

The surface integral approach calculates the corona charge through Gauss's law by integrating the surface field $E_n$ on the aircraft for regions in which the surface field exceeds the corona stabilization field.

Similarly, the volume integral approach computes the corona charge by integrating the divergence of the potential field in a volume outside the surface on which $E > E_{cr}$, as given in Fig. 2. Note that **u** is the normalized electric field on the volume:

$$E = E_{cr}\mathbf{u} \tag{3}$$

It is not useful to integrate over a very large area, as this pollutes the measurement with samples from far-away points. To mitigate this, the domain of integration is restricted to 0.75 times the fuselage radius of the aircraft. This value was used in [2] and yielded satisfactory results.

The following parameters are used in computing the corona charge and leader inception criteria for the results reported in this paper, and are adopted from [3,11,13]:

Table 1.  Physical Parameters used in the Attachment Model

| Parameter | Value |
|---|---|
| Corona charge evaluation | Surface integral |
| $E_{stab}^+$ | 470 kV/m |
| $E_{stab}^-$ | 750 kV/m |
| $Q_{cr}^+$ | $1.0\mu C$ |
| $Q_{cr}^-$ | $4.0\mu C$ |
| $\dfrac{r_{integration}}{R_{fuselage}}$ | 0.75 |

### 4.2 Selection of potential attachment points

The following steps are used to calculate the first leader attachment points for the case of an uncharged aircraft, $Q_{ac}$=0, at a given orientation of the ambient field $E_\infty$. This methodology differs from previous zoning methods because the attachment points are computed automatically without requiring input of a possible list of points beforehand. Also, the model allows for the first attachment point to be either positive or negative. The process is as follows:

1. Determine automatically which points could serve as candidate attachment points. This is done by initializing the background electric field to a low level and sorting the electric field amplitudes at the surface points. A certain number of the points with the greatest amplitude (for a positive leader) and least amplitude (for a negative leader) are taken. In this model, the top 5,000 points each were chosen for the positive and negative leaders.

2. To maintain a reasonable computational cost, we need to limit the number of points at which integrals are performed to a few dozen per sign. However, this cannot be done by a simple thresholding of the surface field because the points with the greatest amplitude may be clustered together in the same vicinity, which would be akin to using the maximum value of the surface field as the attachment criteria. Points with a lower field amplitude elsewhere on the aircraft may have a higher chance of being attachment points depending on the surrounding field. Thus, we must develop a way to include points on different parts of the aircraft while keeping the total number of points low. This is accomplished with a *k*-means

clustering algorithm. *K*-means is an unsupervised classification algorithm that partitions a set of observations into k clusters, with the observations in each cluster sharing the same classification label. Each observation is associated with the cluster with the nearest mean. In this research, k-means clustering is applied to the coordinates of the 5,000 potential attachment points previously identified in order to identify separate regions of the aircraft that contain likely attachment points. In this work, seven clusters were chosen. However, this value can be increased without significant impact on the results.

3. Within each cluster, a small number of points are chosen as the final values on which to run the attachment analysis. For each of the seven clusters, the top three points are selected, resulting in 21 points per leader sign. Such a large number of points (5,000) were chosen in the initial thresholding step because it is possible for many high amplitude points to be clustered together in regions of the aircraft where the mesh resolution is fine, for example at the wingtips, nose, or tail. Without clustering, points with a reasonably high amplitude elsewhere on the surface would not be considered.

## 4.3 First leader inception

With the list of potential attachment points generated, the first leader inception assessment can now be conducted. This process is performed by iteratively updating the magnitude of **E** and checking the corona inception conditions:

1. Initialize the background **E** to a low value, and hold $Q_{ac}$ at 0, as we are interested in leader inception under uncharged conditions. For each possible attachment point computed above, the surface integral of $E_n$ is performed over elements with a field exceeding the sign-respective stabilization field. This yields a corona charge that can be compared to the critical corona charge, $Q_{cr}^{+/-}$.

2. This process is repeated for all potential attachment points of both charge signs. Then, the corona charges are normalized by their respective critical charges, and the corona charge "error" is calculated. Note that the error is positive if the corona charge is greater than the critical charge, for both positive and negative coronae.

$$error = \frac{Q_{calculated,\pm}}{Q_{cr}^{\pm}} - 1 \qquad (4)$$

3. Next, the iteration update is calculated as:

$$E^{n+1} = E^n - sign(error)\Delta E_0 \frac{1}{2}^{sign\ flips} \qquad (5)$$

where $\Delta E_0$ was chosen as $0.5E_{cr}{}^+$, and "sign flips" is the number of times the error crosses 0 (the sign of the error changes), indicating an over- or under-shoot of the setpoint as the error converges to zero.

The sign and magnitude of the increment to **E** depends on how many leaders, and of what sign, are incepted. The stopping condition is met when the error at the current iteration is positive but below a certain threshold, indicating that a leader has been incepted and that the corresponding value of **E** is just great enough for inception but no more.

A successive approximation algorithm is used with a series of increasingly fine updates to **E** as the error converges to $0^+$. Each time the sign of the error changes, the error increment is reduced by one-half as shown in (5).

## 4.4 Second Leader Attachment

When the first leader is incepted, it propagates away from the aircraft in a conductive channel that draws charge away from the surface. In order for the aircraft-leader system to remain neutral, the aircraft becomes increasingly charged to the opposite polarity. After some time, this polarization causes a second leader to be incepted, thus forming a bidirectional leader. The approach makes no attempt to resolve the leader inception process in time, but examines the charge required to incept the second leader. The process is as follows:

1. First leader is incepted at an ambient field level of **E**baseline and $Q_{ac}$=0 using the process described above.

2. $Q_{ac}$ is updated in a similar fashion to **E** in the first attachment scheme until the error for the opposite sign converges to $0^+$.

The point of second leader attachment is recorded when the iteration terminates.

## 4.5 Determining the attachment points

The computations in Sections 4.3 and 4.4 yield a list of first attachment points, differentiated by sign, for the initial and oppositely charged leaders. Since the attachment points are computed automatically, clear attachment zones are not yet defined. For example, the aircraft may have attachment points identified in a cluster surrounding the nose, but those points are not identified as each belonging to the same zone. Thus, a second clustering step is implemented using *k*-means. This time, the user is prompted to specify the number of clusters that can be counted as distinct zones based on a displayed model of the aircraft with the attachment points highlighted. This level of user interaction was deemed acceptable and necessary, as it prevents the mis-classification of attachment zones.

## 4.6 Optimal Charging Strategy

It is widely accepted that the negative leader exhibits a critical corona charge that is several times greater in magnitude than the positive one [2,11,12]. This asymmetry can be exploited to allow the aircraft to sustain higher external fields through an optimal charging strategy. As mentioned above, the positive leader is usually incepted first, followed by the negative leader after a certain amount of positive charge has been removed from the aircraft. By biasing the aircraft to a potential at which inception of the positive and negative leaders is equally likely, the external field required to incept either leader will be higher than the baseline inception field with $Q_{ac}$=0. The optimal aircraft charge is computed at each orientation, and is performed as follows:

1. First leader is incepted at an ambient field level of **E**baseline and $Q_{ac}$=0 using the process described in the previous section.

2. Assess the corona charge at the attachment points of the opposite sign and take the point with the largest error.

3. Increment $Q_{ac}$ by:

$$Q_{ac}^{n+1} = Q_{ac}^n - sign(error^+ - error^-)\Delta Q_0 \frac{1}{2}^{sign\ flips} \qquad (6)$$

where $\Delta Q_0$ was chosen as .1 mC. Repeat at step 1, recalculating the first attachment point and **E**attach. Note that the sign convention for the error is positive if a leader has been incepted of either sign. If |error+ - error-| falls below the

stopping condition, then stop and return the two attachment points, the level of $\mathbf{E_{attach}}$, and $Q_{ac}$ required for simultaneous leader inception at that orientation.

## 5. RESULTS FOR UNCONVENTIONAL AIRCRAFT

The example aircraft used in this work is the MIT D8, or "Double Bubble". This aircraft design was conceived in the late 2000s for the NASA N+3 program [14]. It is intended to be a next generation replacement to commercial subsonic transports, of the same size class as the Boeing 737. Key design objectives are the reduction of noise, fuel burn, and emissions. As a result, the design deviates significantly from conventional transport aircraft, with the placement of the engines at the rear of the fuselage for boundary layer ingestion, the placement of the horizontal stabilizer above the fuselage, and the "double bubble" fuselage cross section. Thus, this configuration is an ideal candidate for illustrating the generalization of the computational zoning methodology to unconventional aircraft geometries.
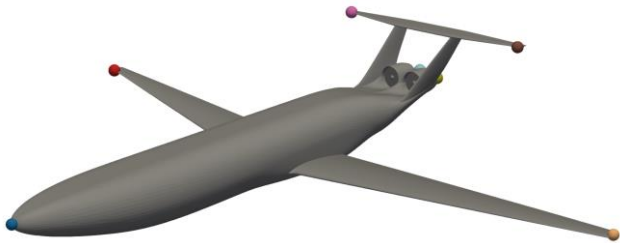


*Figure 3. D8 aircraft with first attachment points overlaid as colored spheres*

The above figure shows the D8 with the attachment points, the output from Section 4.5, highlighted. This represents the aggregated data from the attachment analysis run at every orientation, but it does not convey information about the attachment probability as a function of the electric field orientation. This information is provided below, and the color codes match the aircraft diagram above:
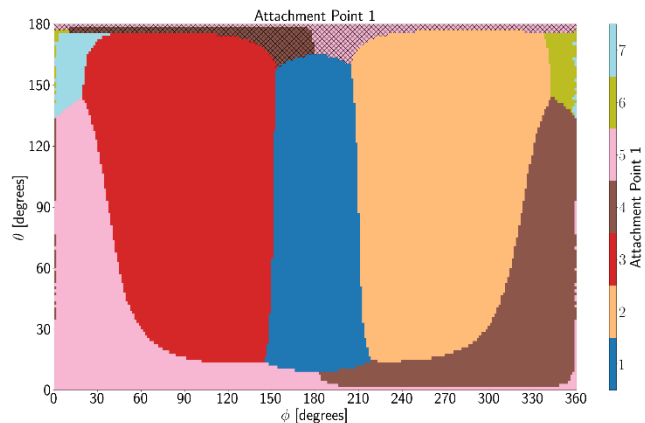


*Figure 4. First attachment map for the D8. The negative first leader attchment points are called out with the hatched pattern.*

Table 2. probabilities for the D8 computed using the surface integral method

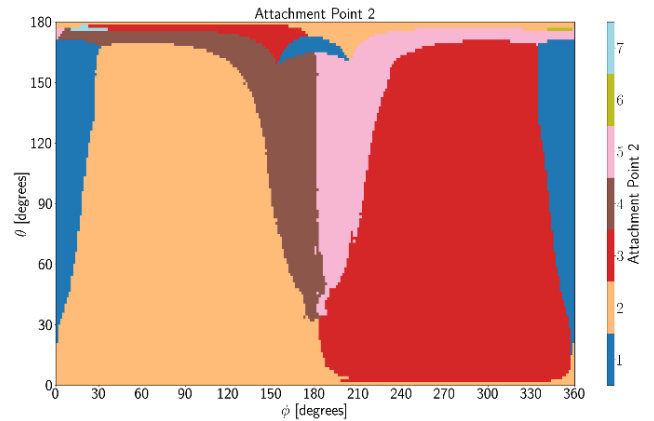| Aircraft Location | Code | Attachment Probability |
|---|---|---|
| Nose | 1 | 15.9 |
| Left Wing | 2 | 30.4 |
| Right Wing | 3 | 30.5 |
| Left Vertical Stabilizer | 4 | 10.7 |
| Right Vertical Stabilizer | 5 | 10.3 |
| Left Engine Exhaust Duct | 6 | 0.6 |
| Right Engine Exhaust Duct | 7 | 0.7 |



*Figure 5. Map of opposite polarity (second) leader attachment for the D8*

The analysis agrees with the computational zoning model presented in [2] qualitatively in regards to attachment point locations. Experimental validation using long arc attachment testing on sub-scale models, as in [2,4], is left to future work. It is observed that the engine exhaust ducts at the rear of the aircraft are classified as attachment points, albeit with a much lower probability than the other features. Of note is that with this geometry, there is no vertical tail serving as an attachment point when the field is oriented vertically, as compared to conventional aircraft. The electric field strength required to incept the first leader is plotted below as a function of orientation.
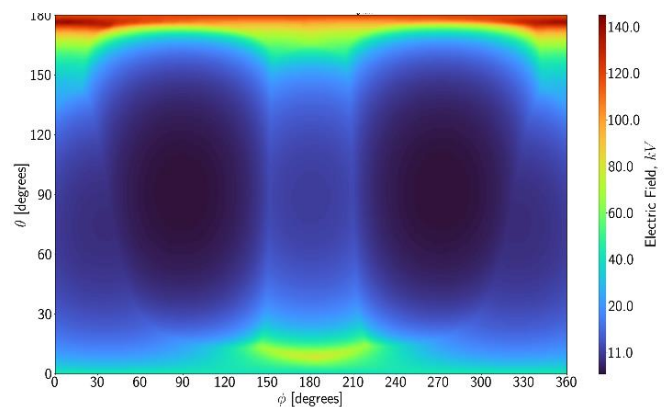


*Figure 6. Breakdown external field levels for the uncharged case as a function of E orientation*

For this case, the optimum charging strategy was also calculated. The plots below show the field margin that the strategy provides, as well as the optimum charge for each orientation. The analysis suggests that with the optimum

charging strategy, this aircraft can sustain fields up to 60% higher than in the baseline uncharged configuration, depending on the orientation of the field.
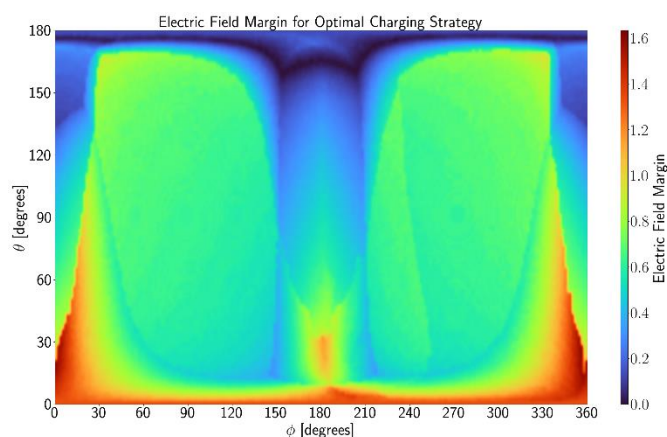


Figure 7. Electric field breakdown margin over the baseline case using the optimal charging strategy
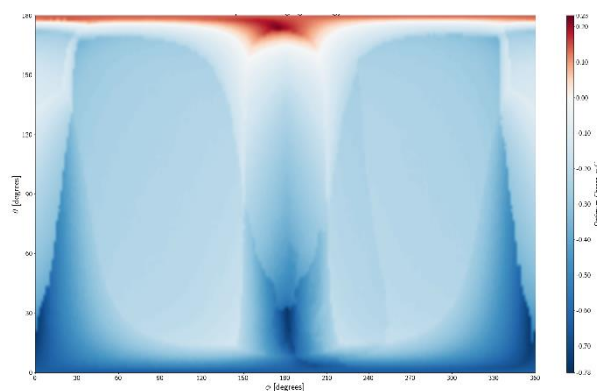


Figure 8. Optimal aircraft charge as a function of electric field orientation, in mC

## CONCLUSIONS

We have produced a tool for the computational zoning of arbitrary aircraft geometries with minimal user intervention. The tool is capable of predicting initial attachment points of either polarity, and of computing the optimal charge to allow the aircraft to sustain the highest possible electric field based upon the asymmetry of positive and negative critical corona charges. An insertion point for this tool is imagined in the early design stage of a new aircraft, where the attachment analysis can be integrated with iteration on the conceptual design of new vehicles. This allows for lightning mitigation to be incorporated from the start, instead of performing the analysis downstream at the time of aircraft certification.

Future work will focus on coupling the attachment model to a sweeping model in order to predict the path that the lightning channel will take across the aircraft as it remains attached during the return stroke period. Already, work is beginning on developing the framework for using this tool with an inviscid flow solution to enable zoning of the time-dependent subsequent attachment points.

## REFERENCES

[1] C. Guerra-Garcia , J. Peraire M. Martinez-Sanchez, N. C. Nguyen. Influence of net charge on the probability of lightning initiation from aircraft, ICOLSE 2017.

[2] C. Guerra-Garcia , J. Peraire M. Martinez-Sanchez, N. C. Nguyen. Charge control strategy for aircraft-triggered lightning strike risk reduction. AIAA Journal, 2018

[3] J. Gokcen G. Sweeters, B. Birch. lightning strikes: Protection, inspection, and repair. https://www.boeing.com/commercial/aeromagazine/articles/2012_q4/4/, 2012

[4] A. Delannoy P. Lalande. Numerical methods for zoning computation. Aerospace Lab Issue 5, December 2012

[5] SAE ARP 5412: Aircraft lightning environment and related test waveforms. Technical report, SAE International, November 1999.

[6] SAE ARP 5414a: Aircraft lightning zoning. Technical report, SAE International, September 2012

[7] H. Kasemir. Static discharge and triggered lightning. Proc. 8th International Aerospace and Ground Conference on Lightning and Static Electricity, June 1963

[8] A. Bondiou-Clergerie P. Lalande and P. Laroche. Computations of the initial discharge initiation zones on aircraft or helicopter. International Conference on Lightning and Static Electricity (ICOLSE), June 1999.

[9] Albert Reuther et al. Interactive supercomputing on 40,000 cores for machine learning and data analysis. In 2018 IEEE High Performance extreme Computing Conference (HPEC), pages 1–6. IEEE, 2018

[10] S. Austin, Implementation of an arbitrary high order 3D Continuous Galerkin Finite Element Method, https://github.com/saustinp/3D-CG

[11] I. Gallimberti. The mechanism of the long spark formation. Journal de Physique, July 1979

[12] I. Gallimberti et al. Fundamental processes in long air gap discharges. 2002

[13] P. Lalande A. Bonamy I. Gallimberti A. Castellani, A. Bondiou-Clergerie. Laboratory study of the bi-leader process from an electrically floating conductor. Part 1 : General results. IEE Proceedings - Science, Measurement and Technology, September 1998

[14] NASA N+3 MIT Team Final Review, NASA Langley Research Center.http://web.mit.edu/drela/Public/N+3/Final_slides.pdf, April 2010.